

NEUTRINOS IN ANOMALY MEDIATED SUPERSYMMETRY BREAKING WITH R -PARITY VIOLATION

F. de Campos^a, M.A. Díaz^b, O.J.P. Éboli^c, R.A. Lineros^b, M.B. Magro^{c,d},
and P.G. Mercadante^c.

^a*Departamento de Física e Química, Universidade Estadual Paulista,
Av. Dr. Ariberto Pereira da Cunha 333, Guaratinguetá, SP, Brazil*

^b*Departamento de Física, Universidad Católica de Chile,
Av. V. Mackenna 4860, Santiago, Chile*

^c*Instituto de Física da USP, C.P. 66.318,
05315-970, São Paulo, Brazil and*

^d*Faculdade de Engenharia, Centro Universitário FSA,
Av. Príncipe de Gales 821, Santo André, SP, Brazil*

Abstract

We show that a supersymmetric standard model exhibiting anomaly mediated supersymmetry breaking can generate naturally the observed neutrino mass spectrum as well mixings when we include bilinear R -parity violation interactions. In this model, one of the neutrinos gets its mass due to the tree level mixing with the neutralinos induced by the R -parity violating interactions while the other two neutrinos acquire their masses due to radiative corrections. One interesting feature of this scenario is that the lightest supersymmetric particle is unstable and its decay can be observed at high energy colliders, providing a falsifiable test of the model.

I. INTRODUCTION

There have been many experimental results in neutrino physics [1] which have established the pattern of neutrino oscillation and masses, clearly requiring physics beyond the standard model (SM) to explain it. In general, neutrino oscillations are parametrized by three mixing angles, with two of them large, as opposed to the quark sector where the mixing angles are all small. Moreover, neutrino oscillations depend also on the mass squared differences, and we have learned that the mass difference corresponding to the atmospheric neutrino oscillations is much larger than the corresponding one to the solar neutrino oscillations [1]. The analysis of the solar neutrinos leads to the 3σ level limits [2] (see also [3])

$$\begin{aligned} 0.23 &\lesssim \sin^2 \theta_{\text{sol}} \lesssim 0.37 \\ 7.3 \times 10^{-5} &\lesssim \Delta m_{\text{sol}}^2 \lesssim 9.1 \times 10^{-5} \text{ eV}^2 \end{aligned} \quad (1.1)$$

while the atmospheric neutrino data shows that

$$\begin{aligned} 0.34 &\lesssim \sin^2 \theta_{\text{atm}} \lesssim 0.66 \\ 1.4 \times 10^{-3} &\lesssim \Delta m_{\text{atm}}^2 \lesssim 3.3 \times 10^{-3} \text{ eV}^2 . \end{aligned} \quad (1.2)$$

Despite the lack of direct experimental evidence on supersymmetry (SUSY), supersymmetric models are promising candidates for physics beyond the SM. It is an experimental fact that SUSY must be broken if it is realized in nature. Here, we consider the anomaly-mediated SUSY breaking scenario (AMSB) where the supersymmetry breaking in the hidden sector is transmitted into the observable sector by the Super-Weyl anomaly [4]. Below the compactification scale, the model is described by an effective four dimensional supergravity theory, where the soft supersymmetry breaking parameters are generated beyond tree level. Without further contributions the slepton squared masses turn out to be negative. This tachyonic slepton problem can be solved by adding a common scalar mass to all scalars [5].

It has been suggested a long time ago that supersymmetry and neutrino masses and mixings may be deeply tied together [6]. One way of giving mass to the neutrinos in supersymmetric models is via Bilinear R -Parity Violation (BRpV): in such model, bilinear terms which violates lepton number as well as R -Parity are introduced in the superpotential [7, 8, 9]. As a consequence, one neutrino acquires mass at tree level due to a low energy see-saw mechanism in which neutrinos mix with neutralinos. The other two neutrinos become massive via one-loop corrections to the neutralino-neutrino mass matrix [10].

It has been shown that BRpV can be successfully embedded into models with AMSB [11] giving rise at tree level to a neutrino mass compatible with the atmospheric neutrino mass scale. Here, we generalize this model including lepton number violating interaction in the three generations and we show that the inclusion of one-loop corrections to the neutralino–neutrino mass matrix leads to a neutrino spectrum and mixings compatible with the available data. This is non-trivial since the radiative corrections depend on the SUSY spectrum and it is not clear *a priori* that the corrections will have the required properties after we impose the existing limits on the SUSY mass spectrum.

This paper is organized as follows. In Section II we briefly show the principles of the AMSB-BRpV model. In Section III we discuss the effects of BRpV on the neutrino mass and mixing angles. In Section IV we present our reference scenario and its main properties. The results for an AMSB model exhibiting BRpV are presented in Section V and we conclude in Section VI.

II. THE AMSB–BRPV MODEL

The superpotential of our BRpV model includes three ϵ_i parameters with units of mass not present in the MSSM [7, 12]

$$W = W_Y - \mu \widehat{H}_d \widehat{H}_u + \epsilon_i \widehat{L}_i \widehat{H}_u, \quad (2.1)$$

with W_Y including the Yukawa interactions. The ϵ terms violate lepton number and R -Parity and satisfy $|\epsilon_i| \ll \mu$. The appearance of R -Parity violating bilinear terms and not trilinear terms can be justified in models with a horizontal symmetry [13], or in models with spontaneous R -Parity breaking [14]. In addition to the ϵ_i terms in the superpotential, we must add the soft lagrangian bilinear terms proportional to $B_i \epsilon_i$. For our purposes the relevant terms are

$$V_{soft} \ni -B\mu H_d H_u + B_i \epsilon_i L_i H_u + m_{H_d}^2 H_d^* H_d + m_{L_i}^2 \widetilde{L}_i^* \widetilde{L}_i. \quad (2.2)$$

In principle, it is possible to redefine the superfields in order to make BRpV terms disappear from the superpotential, however, they do not vanish from the soft lagrangian simultaneously [15].

The scalar potential of BRpV models is such that the sneutrino fields acquire a non zero vacuum expectation value v_i that leads to the generation of neutrino mass and mixing angles.

Even in the basis where the ϵ_i terms are removed from the superpotential, the sneutrino fields acquire non-zero vev's $v'_i \approx (\epsilon_i v_d + \mu v_i)/\mu$ [10] which, from the minimization of the scalar potential, can be shown to satisfy

$$v'_i \approx 2v_d \frac{\epsilon_i}{\mu} \frac{\Delta m_i^2 - \mu \Delta B_i \tan \beta}{2M_{L_i}^2 + m_Z^2 \cos(2\beta)} \quad (2.3)$$

with $\Delta m_i^2 = M_{L_i}^2 - m_{H_d}^2$ and $\Delta B_i = B_i - B$. Since there is no reason to assume that these differences are zero *at the weak scale*, the sneutrino vev's are not zero either.

The parameters defining our BRpV-AMSB model are the usual ones in AMSB models

$$m_0, \quad m_{3/2}, \quad \tan \beta, \quad \text{and} \quad \text{sign}(\mu), \quad (2.4)$$

where the scalar mass m_0 and the gravitino mass $m_{3/2}$ are given at the unification scale. This set of parameters is supplemented by the six BRpV parameters ϵ_i and B_i . It is advantageous to trade B_i by a parameter more directly connected to the neutrino physics observables, therefore, we shall choose the parameters Λ_i defined below instead of B_i as input parameters. One of the virtues of AMSB models is that the $SU(2) \otimes U(1)$ symmetry is broken radiatively by the running of the parameters from the GUT scale to the weak one. This feature is preserved in our model exhibiting BRpV.

III. NEUTRINO AND NEUTRALINO MASSES

In the basis $\psi^{0T} = (-i\lambda', -i\lambda^3, \widetilde{H}_d^1, \widetilde{H}_u^2, \nu_e, \nu_\mu, \nu_\tau)$ the 7×7 neutral fermion mass matrix M_N has the see-saw structure, at tree level,

$$M_N = \begin{bmatrix} \mathcal{M}_{\chi^0} & m^T \\ m & 0 \end{bmatrix}, \quad (3.1)$$

where the standard MSSM neutralino mass matrix is

$$\mathcal{M}_{\chi^0} = \begin{bmatrix} M_1 & 0 & -\frac{1}{2}g'v_d & \frac{1}{2}g'v_u \\ 0 & M_2 & \frac{1}{2}gv_d & -\frac{1}{2}gv_u \\ -\frac{1}{2}g'v_d & \frac{1}{2}gv_d & 0 & -\mu \\ \frac{1}{2}g'v_u & -\frac{1}{2}gv_u & -\mu & 0 \end{bmatrix}, \quad (3.2)$$

and R -parity violating interactions give rise to sneutrino vev's and mixings between neutrinos and gauginos/higgsinos:

$$m = \begin{bmatrix} -\frac{1}{2}g'v_1 & \frac{1}{2}gv_1 & 0 & \epsilon_1 \\ -\frac{1}{2}g'v_2 & \frac{1}{2}gv_2 & 0 & \epsilon_2 \\ -\frac{1}{2}g'v_3 & \frac{1}{2}gv_3 & 0 & \epsilon_3 \end{bmatrix} . \quad (3.3)$$

Due to its structure M_N exhibits just one massive neutrino at tree level while the other two remain massless. The degeneracy of these two states is lifted when we include the one-loop corrections to the neutral fermion mass matrix.

In order to get some intuition on the main effects of BRpV, it is instructive to analyze the limit $|\epsilon_i| \ll \mu$ where we can perform a perturbative diagonalization of the neutralino-neutrino mass matrix in terms of the parameters [7]

$$\xi \equiv m \cdot \mathcal{M}_{\chi^0}^{-1} . \quad (3.4)$$

In this approximation M_N is diagonalized by the rotation matrix

$$\mathcal{N}^* \simeq \begin{pmatrix} N^* & N^*\xi^\dagger \\ -V_\nu^T \xi & V_\nu^T \end{pmatrix} , \quad (3.5)$$

where N^* diagonalizes the 4×4 neutralino mass matrix \mathcal{M}_{χ^0} and V_ν diagonalizes the effective tree level neutrino mass matrix

$$\mathbf{M}^{\text{eff}} = -m \mathcal{M}_{\chi^0}^{-1} m^T . \quad (3.6)$$

Within this approximation [10], it can be shown that the atmospheric mass scale is adequately described by the tree level neutrino mass

$$m_{\nu_3}^{\text{tree}} = \frac{M_1 g^2 + M_2 g'^2}{4\Delta_0} |\vec{\Lambda}|^2 , \quad (3.7)$$

where Δ_0 is the determinant of the neutralino sub-matrix \mathcal{M}_{χ^0} and $\vec{\Lambda} = (\Lambda_1, \Lambda_2, \Lambda_3)$, with

$$\Lambda_i = \mu v_i + \epsilon_i v_d \approx \mu v'_i , \quad (3.8)$$

and the index i refers to the lepton family. Due to this direct relation between neutrino mass and Λ_i , from now on, we eliminate the B_i as independent parameters in favor of Λ_i .

Moreover, the mixing angles between the massive neutrino state and the tree level massless ones are given approximately by

$$\tan \theta_{13} = -\frac{\Lambda_1}{\sqrt{\Lambda_2^2 + \Lambda_3^2}} \quad \text{and} \quad \tan \theta_{23} = -\frac{\Lambda_2}{\Lambda_3}. \quad (3.9)$$

The one-loop corrections to the neutralino–neutrino mass matrix in the presence of BRpV interactions have been evaluated in Refs. [10]. The mixing of neutrinos with gauginos and higgsinos due to BRpV leads to effective interactions neutrino–quark–squark and neutrino–lepton–slepton. These vertices give rise to squark–quark and slepton–lepton loop contributions to the neutrino mass matrix that are proportional to the R –Parity violating parameters, vanishing when R –Parity is conserved [10]. In the approximation that only the bottom quark–bottom squark loop gives a sizeable contribution to the one-loop corrections to the neutrino masses [16], the scale of the solar neutrino mass is given by

$$m_{\nu_2} \propto \frac{|\vec{\epsilon}|^2}{16\pi^2\mu^2} m_b, \quad (3.10)$$

while the solar mixing angle is

$$\tan \theta_{12} \simeq \left| \frac{\tilde{\epsilon}_1}{\tilde{\epsilon}_2} \right| \quad \text{where} \quad \tilde{\epsilon}_i = V_{ij}^{\nu, \text{tree}} \epsilon_j. \quad (3.11)$$

Still within this approximation we have

$$\begin{aligned} \tilde{\epsilon}_1 &= \frac{\epsilon_1(\Lambda_2^2 + \Lambda_3^2) - \Lambda_1(\Lambda_2\epsilon_2 + \Lambda_3\epsilon_3)}{\sqrt{\Lambda_2^2 + \Lambda_3^2} \sqrt{\Lambda_1^2 + \Lambda_2^2 + \Lambda_3^2}}, \\ \tilde{\epsilon}_2 &= \frac{\Lambda_3\epsilon_2 - \Lambda_2\epsilon_3}{\sqrt{\Lambda_2^2 + \Lambda_3^2}}, \\ \tilde{\epsilon}_3 &= \frac{\vec{\Lambda} \cdot \vec{\epsilon}}{\sqrt{\Lambda_1^2 + \Lambda_2^2 + \Lambda_3^2}}. \end{aligned} \quad (3.12)$$

These approximations are valid when the tree level contribution is dominant and one-loop contributions are small corrections. However, this is not always true as we will see in the next sections. In this case, the above formulas are no longer valid.

IV. REFERENCE SCENARIO

In order to understand the main features of our model, we considered a point in the parameter space which satisfies all the collider and neutrino physics constraints and then

explore the parameter space around it. First, we choose an AMSB scenario in which all superpartner masses satisfy the present experimental bounds and where we obtain a correct electroweak symmetry breaking; we used the code SUSPECT [17] to compute the two-loop running of the parameters from the GUT scale to the weak one. At this scale, the minimization of the scalar potential is generalized to include five vacuum expectation values: v_u and v_d for the Higgs fields and v_i for the sneutrinos. For the AMSB parameters, see experimental restrictions on the parameters in [18], we chose

$$m_{3/2} = 35 \text{ TeV}, \quad m_0 = 250 \text{ GeV}, \quad \tan\beta = 15, \quad \text{and} \quad \text{sign}(\mu) < 0. \quad (4.1)$$

Second, we randomly varied the parameters ϵ_i and Λ_i looking for solutions in which the restrictions (1.1) and (1.2) from neutrino physics are satisfied. An example of these solutions is

$$\begin{aligned} \epsilon_1 &= -0.015 \text{ GeV}, & \Lambda_1 &= -0.03 \text{ GeV}^2, \\ \epsilon_2 &= -0.018 \text{ GeV}, & \Lambda_2 &= -0.09 \text{ GeV}^2, \\ \epsilon_3 &= 0.011 \text{ GeV}, & \Lambda_3 &= -0.09 \text{ GeV}^2. \end{aligned} \quad (4.2)$$

Eqs. (4.1) and (4.2) define what we call our reference model. The neutrino parameters obtained in this reference model are

$$\begin{aligned} \Delta m_{\text{atm}}^2 &= 2.4 \times 10^{-3} \text{ eV}^2, & \tan^2 \theta_{\text{atm}} &= 0.72, \\ \Delta m_{\text{sol}}^2 &= 7.9 \times 10^{-5} \text{ eV}^2, & \tan^2 \theta_{\text{sol}} &= 0.47, \\ & & \tan^2 \theta_{13} &= 0.033, \end{aligned} \quad (4.3)$$

which agree with the present experimental results.

The effective neutrino mass matrix in our reference model has the structure

$$\mathbf{M}^{\text{eff}} = \begin{bmatrix} \lambda & 2\lambda & \lambda \\ 2\lambda & a & b \\ \lambda & b & m \end{bmatrix}, \quad (4.4)$$

where $m \approx 0.031 \text{ eV}$ sets the overall scale, $a/m \approx 0.74$, $b/m \approx 0.67$, and $\lambda/m \approx 0.12 - 0.14$. As a first approximation, we can neglect the effect of λ and estimate the two heavier neutrino masses

$$m_{\nu_{2,3}} = \frac{1}{2} \left[m + a \pm \sqrt{(m - a)^2 + 4b^2} \right] \quad (4.5)$$

with the lightest neutrino being nearly massless. Numerically, the approximation in Eq. (4.5) leads to $\Delta m_{\text{atm}}^2 \approx 2.3 \times 10^{-3} \text{eV}^2$ which is very close to the complete result given in Eq. (4.3). Still within this approximation, the atmospheric mixing angle satisfy

$$\tan 2\theta_{\text{atm}} \approx \frac{2b}{m-a} \quad (4.6)$$

which leads $\tan^2 \theta_{\text{atm}} \approx 0.68$, also in close agreement with the complete result shown in Eq. (4.3). However, for the solar mass difference, the $\lambda = 0$ approximation is not good giving near half the correct value in Eq. (4.3).

In general, the effective neutrino mass matrix at one-loop has the approximated form [16]

$$\mathbf{M}_{ij}^{\text{eff}} = A\Lambda_i\Lambda_j + B(\epsilon_i\Lambda_j + \epsilon_j\Lambda_i) + C\epsilon_i\epsilon_j, \quad (4.7)$$

where the coefficient A receives tree-level as well as one-loop contributions, and B and C are one-loop generated. Approximated expressions for the contributions from bottom/sbottom and charged-scalar/charged-fermion loops to the parameters A , B and C can be found in [16]. For our reference model, we have $A \approx 3 \text{ eV/GeV}^4$, $B \approx -2 \text{ eV/GeV}^3$, and $C \approx 15 \text{ eV/GeV}^2$. Therefore, for our reference point, the one-loop generated parameters B and C are not negligible, stressing the necessity of using one-loop corrected expressions.

Some of the entries in the effective neutrino mass (4.7) are numerically small for our reference model, which allow us to write as a good first approximation that

$$\mathbf{M}^{\text{eff}} = \begin{bmatrix} A\Lambda_1^2 + 2B\Lambda_1\epsilon_1 + C\epsilon_1^2 & \cdot & \cdot \\ A\Lambda_1\Lambda_2 + B(\epsilon_1\Lambda_2 + \epsilon_2\Lambda_1) + C\epsilon_1\epsilon_2 & A\Lambda_2^2 + 2B\epsilon_2\Lambda_2 & \cdot \\ A\Lambda_1\Lambda_3 + C\epsilon_1\epsilon_3 & A\Lambda_2\Lambda_3 & A\Lambda_3^2 + 2B\epsilon_3\Lambda_3 \end{bmatrix}, \quad (4.8)$$

where the matrix is symmetrical and we do not repeat the redundant terms. From this expression, it can be shown, neglecting the first row and the first column, that the atmospheric angle is given by

$$\tan 2\theta_{\text{atm}} = \frac{2A\Lambda_2\Lambda_3}{A(\Lambda_3^2 - \Lambda_2^2) + 2B(\epsilon_3\Lambda_3 - \epsilon_2\Lambda_2)}. \quad (4.9)$$

Since only A receives contributions at tree-level, it is no surprise that the above formula approaches the tree-level expression in Eq. (3.9) when $B \rightarrow 0$. Nevertheless, as we have seen, the one-loop corrections to B are non-negligible in our reference model, leading to departures from the naïve expectations. Moreover, we can also demonstrate that the masses

of the two heaviest neutrinos are approximated by

$$m_{\nu_{2,3}} = \frac{1}{2}A(\Lambda_3^2 + \Lambda_2^2) + B(\epsilon_3\Lambda_3 + \epsilon_2\Lambda_2) \pm \sqrt{\left[\frac{1}{2}A(\Lambda_3^2 - \Lambda_2^2) + B(\epsilon_3\Lambda_3 - \epsilon_2\Lambda_2)\right]^2 + A^2\Lambda_2^2\Lambda_3^2} , \quad (4.10)$$

while the lightest neutrino mass is negligible. Since the values of ϵ_2 and ϵ_3 are much smaller than $\Lambda_2 = \Lambda_3$ in our reference model, the A term gives rise to the most important contribution. The two neutrino masses in Eq. (4.10) are hierarchical, therefore the squares of m_{ν_3} and m_{ν_2} are a good first approximation to the atmospheric and solar mass squared differences.

V. RESULTS

Let us initially analyze the dependence of the neutrino masses and mixings upon the AMSB parameters. In Fig. 1 it is shown the dependence on the scalar mass m_0 of the predicted atmospheric neutrino mass squared difference Δm_{atm}^2 (red solid line) and the solar neutrino mass squared difference Δm_{sol}^2 (blue dashed line), for fixed values $m_{3/2} = 35$ TeV, $\tan\beta = 15$, and $\text{sign}(\mu) < 0$ and for the BRpV parameters given in (4.2). As we can see from this figure, Δm_{atm}^2 is a decreasing function of m_0 while Δm_{sol}^2 has a more complex behavior.

When the scalar mass m_0 increases the masses of the scalar SUSY particles grow, and consequently, decoupling effects make the A term to diminish. In fact all three terms m , a , and b in the texture (4.4) decrease with m_0 . This explains why the atmospheric mass decreases monotonically with m_0 in Fig. 1. Nevertheless, this phenomenon does not happen for the solar mass due to the minus sign in Eq. (4.10) which causes the complex behavior. For instance, at large m_0 the square root decreases a slightly faster than the term outside the square root, increasing the solar mass as observed in Fig. 1.

We can also see from Fig. 1 that Δm_{atm}^2 is within the present experimental bounds for $m_0 \lesssim 1.6$ TeV while Δm_{sol}^2 satisfies the experimental constraints for $m_0 \lesssim 310$ GeV and 1.4 TeV $\lesssim m_0 \lesssim 1.75$ TeV. Therefore, our models lead to acceptable neutrino masses provided $m_0 \lesssim 310$ GeV or 1.4 TeV $\lesssim m_0 \lesssim 1.6$ TeV for all other parameters fixed at their reference values. It is also important to notice that the heaviest neutrino state has a mass of the order of 0.050 eV for our reference point and that it decreases as m_0 increases. Moreover, the radiative corrections lead to a contribution of $\mathcal{O}(10\%)$, therefore, the tree-level result

for the neutrino mass is a good order of magnitude estimative.

We depict in Fig. 2 the tangent squared of the atmospheric (solar) angle $\tan^2 \theta_{\text{atm(sol)}}$ as a function of m_0 for our reference point. As we can see from this figure, there is a small dependence on m_0 of the atmospheric mixing angle and a milder one of the solar mixing. Due to the importance of one-loop corrections, the lowest order approximated expressions (3.9) and (3.11) do not describe the dependence of the solar and atmospheric mixings on the scalar mass m_0 ; in order to understand this behavior we should use the full one-loop approximation (4.9). For $\Lambda_2 = \Lambda_3$, this expression reduces to

$$\tan 2\theta_{\text{atm}} = \frac{A\Lambda_3}{B(\epsilon_3 - \epsilon_2)}. \quad (5.1)$$

We checked that there is a clear decrease of the parameter A with m_0 , while B slightly increases, explaining the slope in the atmospheric angle curve. We verified further that a similar effect happens for $m_{3/2}$, *i.e.*, a very mild dependence of the solar angle and a slight decrease of $\tan^2 \theta_{\text{atm}}$ with increasing $m_{3/2}$, since its tree level contribution to A is inversely proportional to the gaugino masses. Note from Eqs. (4.9) and (5.1) that the fact that ϵ_2 and ϵ_3 have different signs is responsible for preventing the atmospheric angle to be maximal since $\Lambda_2 = \Lambda_3$ in our reference model.

In Fig. 3 we display the dependence of the atmospheric and solar mass squared differences on the gravitino mass $m_{3/2}$ for the other parameters assuming their reference values. First of all, the observed dependence is much stronger compared to the dependence on m_0 ; this is expected due to the large impact of $m_{3/2}$ on the soft gaugino masses, which together with μ define the tree-level neutrino mass matrix. Moreover, the SUSY spectrum has a large impact on the one-loop corrections increasing the sensitivity to $m_{3/2}$. Both solar and atmospheric squared mass differences are too large in the region of small gravitino masses, however, this region is already partially ruled out since it leads to charginos lighter than the present experimental bounds for $m_{3/2} \lesssim 30$ TeV. Conversely, there is no acceptable solution for the neutrino masses at large $m_{3/2}$, again a region partially ruled out by data since the staus are too light in this region. Furthermore, we can see from this figure that our AMSB-BRpV model leads to acceptable neutrino masses for a small window of the gravitino mass ($33 \text{ TeV} \lesssim m_{3/2} \lesssim 36 \text{ TeV}$) given our choice of parameters. This is far from trivial since we have no *a priori* guaranty that we can generate the required neutrino spectrum, specially the radiative corrections, satisfying at the same time the experimental constraints on the

superpartner masses.

In Fig. 4 we present Δm_{atm}^2 and Δm_{sol}^2 as a function of $\tan\beta$ with all other parameters fixed at their reference values. Clearly, Δm_{atm}^2 has a very mild dependence upon $\tan\beta$ since it is dominated by the tree level contributions. Nevertheless, Δm_{sol}^2 presents a strong dependence on this parameter, exhibiting an acceptable solution only for a very narrow range $14.8 \lesssim \tan\beta \lesssim 15.3$. This is a consequence of the strong dependence of the radiative corrections on $\tan\beta$. The effective interaction $\nu b\tilde{b}$ generated after the diagonalization of the neutralino–neutrino mass matrix has a coupling λ'_{333} that exhibits a term proportional to $\tan\beta$, leading to the observed strong dependence. In other words, the neutrino mixes with the higgsino, which couples to bottom-sbottom via the bottom Yukawa coupling which increases with $\tan\beta$. At large $\tan\beta$, the lightest stau become lighter than the present experimental bounds, therefore, this region is already experimentally excluded.

The neutrino masses and mixings present a rich structure when we vary the BRpV parameters. We display in Fig. 5 the neutrino masses as a function of ϵ_2 keeping all other parameters fixed at the reference value; the smallest mass eigenvalue is not displayed and it is usually smaller than 5×10^{-5} eV. As we can see, there is one eigenvalue of the effective neutrino mass matrix that is approximately constant since it is associated to the tree level neutrino mass. However, as $|\epsilon_2|$ grows the radiative corrections start to become important and even to dominate; we observe the same behavior of the neutrino masses with ϵ_1 and ϵ_3 . This is the origin of the level crossing that we see in this figure.

Fig. 6 presents the dependence on ϵ_2 of the predicted atmospheric neutrino squared mass difference Δm_{atm}^2 (red solid line) and the solar neutrino squared mass difference Δm_{sol}^2 (blue dashed line) for all other parameters fixed at the reference values. The cusps we observe in this figure are due to the crossing of eigenvalues of the effective neutrino mass matrix and the fact that we order the neutrino masses $m_{\nu_1} < m_{\nu_2} < m_{\nu_3}$. Moreover, it is clear from this figure that the solar neutrino squared mass difference excludes a larger fraction of the parameter space than the corresponding atmospheric difference; not only the solar squared mass difference is more precisely known, but also the radiative corrections exhibit a strong dependence on ϵ_2 . Nevertheless, there are still two regions where both constraints are satisfied simultaneously. In the region of this figure where the values of $|\epsilon_2|$ are small we can understand the observed dependence on ϵ_2 : The key element is the fact that the term dependent on B in the square root in Eq. (4.10) is numerically smaller than the term

dependent on A . When this condition is fulfilled the following approximated expressions for the two heaviest neutrinos are valid for $\Lambda_2 = \Lambda_3$

$$m_{\nu_{2,3}} \simeq A\Lambda_3^2 + B\Lambda_3(\epsilon_3 + \epsilon_2) \pm A\Lambda_3^2, \quad (5.2)$$

and as before, we approximate the atmospheric and the solar mass differences by $m_{\nu_3}^2$ and $m_{\nu_2}^2$ respectively. In this way, the quadratic growing of the solar mass with ϵ_2 is clear, and the quadratic decreasing of the atmospheric mass is also clear knowing that the term proportional to A is positive and larger than the negative term proportional to B .

We display in Fig. 7 the mixings $\tan^2 \theta_{\text{atm(sol,13)}}$ as a function of ϵ_2 for our reference point. Once again, we can see clearly the crossing of the eigenvalues of the effective neutrino mass matrix that leads to the cusps in this figure. Furthermore, we observe a sharp peak on the solar angle at small values of ϵ_2 which is well explained by Eq. (3.11) that predicts that $\tan \theta_{\text{sol}}$ diverges for $\epsilon_2 = \epsilon_3 \Lambda_2 / \Lambda_3$, *i.e.* $\epsilon_2 = \epsilon_3 = 0.011$ GeV for our reference point. The one-loop approximation (3.11) also describes well the solar mixing for our reference point predicting that $\tan^2 \theta_{\text{sol}} \simeq 0.43$. Conversely, the behavior of $\tan \theta_{\text{atm}}$ with ϵ_2 is well described by the approximated expression (5.1) which predicts $\tan^2 \theta_{\text{atm}} = 0.68$ (1) for our reference point ($\epsilon_2 = \epsilon_3$). Lastly, radiative corrections are also important for $\tan^2 \theta_{13}$ to satisfy the CHOOZ bounds since, for our reference point, the tree-level prediction is $\tan^2 \theta_{13} \simeq 0.06$; too close to the CHOOZ bound.

Fig. 8 contains the neutrino mass square differences as a function of Λ_3 for all other parameters fixed at the reference value; the behavior of Δm^2 is similar for Λ_1 and Λ_2 . In this case there is no neutrino mass eigenvalue crossing which reflects in the absence of cusps in this figure. Moreover, we can see that the atmospheric mass squared difference is much more sensitive to Λ_3 since it receives a large tree-level contribution.

We present in Fig. 9 the mixing angles as a function of Λ_3 for our reference point. Once again, the sharp peak in $\tan^2 \theta_{\text{sol}}$ is well explained by Eq. (3.11) that predicts the peak at $\Lambda_3 = \Lambda_2 \epsilon_3 / \epsilon_2$, *i.e.* $\Lambda_3 = 0.055$ GeV² for our reference point. Another interesting feature of this Figure is the peak in $\tan \theta_{\text{atm}}$ which is not predicted neither by the tree-level approximation (3.9) nor the approximated expression taking into account one-loop effects (4.9). This can be understood as follows. In the approximated formula Eq. (4.9) we neglected terms that are small for our reference point. If $|\Lambda_3|$ is decreased, some of the neglected terms in the 3,2 entry of \mathbf{M}^{eff} , see Eq. (4.8), are no longer negligible. A better

approximation for the atmospheric angle is, in this case,

$$\tan 2\theta_{\text{atm}} = \frac{2A\Lambda_2\Lambda_3 + 2B(\epsilon_3\Lambda_2 + \epsilon_2\Lambda_3)}{A(\Lambda_3^2 - \Lambda_2^2) + 2B(\epsilon_3\Lambda_3 - \epsilon_2\Lambda_2)}. \quad (5.3)$$

which predicts a peak for $\tan \theta_{\text{atm}}$ at

$$\Lambda_3 \approx \frac{-B\epsilon_3\Lambda_2}{A\Lambda_2 + B\epsilon_2} \sim 0.01 \text{ GeV}^2 \quad (5.4)$$

which agrees very well with the numerical result. Clearly the peaks in this figure signals the necessity of using the full neutrino effective mass matrix, as well as the importance of the radiative corrections.

VI. DISCUSSION

In this previous section we showed that an AMSB model with bilinear R -parity violation is viable, *i.e.* we exhibit a region of the parameter space where the model predicts neutrino masses and mixings in agreement with the experimental data as well as the superpartner masses are heavier than the available experimental constraints. Certainly, the most challenging point for this class of models is to generate a solar neutrino mass squared difference in agreement with data since $\Delta m_{\text{solar}}^2$ is due to radiative corrections that depend strongly on the superpartners masses. On the other hand, the connection between the SUSY spectrum, R -parity violating parameters and neutrino properties allow us to directly probe this class of models in collider experiments because the R -parity violating interactions not only might lead to a decay inside the detector of the lightest SUSY particle (LSP), but also it can originate new decay channels for the other superpartners. Furthermore, more precise determinations of the neutrino masses and mixing angles can be also used to falsify this kind of models due to sensitivity of the solar parameters to radiative corrections, and hence to the model parameters. For instance, our reference point can be ruled out by improved limits, or an actual measurement, of $\tan \theta_{13}$.

In the AMSB-BRpV framework, the lightest neutralino presents leptonic decays $\tilde{\chi}_1^0 \rightarrow \nu\ell^+\ell'^-$, semi-leptonic ones $\tilde{\chi}_1^0 \rightarrow \nu q\bar{q}$ or $lq\bar{q}$, and the invisible mode $\tilde{\chi}_1^0 \rightarrow \nu\nu\nu$. If its decay occurs inside the detector we have to take into account new topologies in the search for SUSY since the missing transverse energy is reduced in this scenario as well as there is a larger production of leptons and jets [19]. In addition to that, the LSP can give rise to displaced

vertices which can be used as a smoking gun for SUSY [20]; see [21] for more studies relating neutrino and collider physics. Moreover, in the case of AMSB the lightest neutralino and chargino are almost degenerate, implying that the R -parity violating interactions may play an important role in the decay of the lightest chargino ($\tilde{\chi}_1^\pm$). The possible new $\tilde{\chi}_1^\pm$ decays induced by BRpV are

$$\begin{aligned}
\tilde{\chi}_1^\pm &\rightarrow \bar{q}q'\nu_i, \\
\tilde{\chi}_1^\pm &\rightarrow \ell^\pm q\bar{q}, \\
\tilde{\chi}_1^\pm &\rightarrow \ell_i^+ \ell_j^- \ell_k^\pm, \\
\tilde{\chi}_1^\pm &\rightarrow \ell_i^\pm \nu_j \nu_k,
\end{aligned}
\tag{6.1}$$

where $\ell_i = e, \mu, \tau$. In order to assess the importance of these new signatures for AMSB further detailed studies are needed [22].

Acknowledgments

This work was supported in part by **Conicyt grant No. 1040384**, by Conselho Nacional de Desenvolvimento Científico e Tecnológico (CNPq), and by Fundação de Amparo à Pesquisa do Estado de São Paulo (FAPESP).

-
- [1] Q. R. Ahmad *et al.* [SNO Collaboration], Phys. Rev. Lett. **89**, 011302 (2002); S. Fukuda *et al.* [Super-Kamiokande Collaboration], Phys. Lett. B **539**, 179 (2002); Phys. Rev. Lett. **81**, 1562 (1998); K. Eguchi *et al.* [KamLAND Collaboration], Phys. Rev. Lett. **90**, 021802 (2003); M. H. Ahn *et al.* [K2K Collaboration], Phys. Rev. Lett. **90**, 041801 (2003).
 - [2] M. Maltoni, T. Schwetz, M. A. Tortola and J. W. F. Valle, Phys. Rev. D **67**, 013011 (2003); arXiv:hep-ph/0405172; M. C. Gonzalez-García and Y. Nir, Rev. Mod. Phys. **75**, 345 (2003).
 - [3] H. Nunokawa, W. J. C. Teves and R. Zukanovich Funchal, Phys. Lett. B **562** (2003) 28; P. C. de Holanda and A. Y. Smirnov, JCAP **0302** (2003) 001; P. Aliani, V. Antonelli, M. Picariello and E. Torrente-Lujan, Phys. Rev. D **69** (2004) 013005; J. N. Bahcall, M. C. Gonzalez-Garcia and C. Pena-Garay, JHEP **0302** (2003) 009; G. L. Fogli, E. Lisi, A. Marrone, D. Montanino, A. Palazzo and A. M. Rotunno, Phys. Rev. D **67** (2003) 073002; V. Barger and D. Marfatia,

- Phys. Lett. B **555** (2003) 144; A. Bandyopadhyay, S. Choubey, R. Gandhi, S. Goswami and D. P. Roy, Phys. Lett. B **559** (2003) 121.
- [4] L. Randall and R. Sundrum, Nucl. Phys. B **557**, 79 (1999); G. F. Giudice, M. A. Luty, H. Murayama and R. Rattazzi, JHEP **9812**, 027 (1998).
- [5] A. Pomarol and R. Rattazzi, JHEP **9905**, 013 (1999); T. Gherghetta, G. F. Giudice and J. D. Wells, Nucl. Phys. B **559**, 27 (1999); D. E. Kaplan and G. D. Kribs, JHEP **0009**, 048 (2000).
- [6] C. S. Aulakh and R. N. Mohapatra, Phys. Lett. B **119**, 13 (1982); L. J. Hall and M. Suzuki, Nucl. Phys. B **231**, 41 (1984); G. G. Ross and J. W. F. Valle, Phys. Lett. B **151**, 375 (1985); J. R. Ellis, G. Gelmini, C. Jarlskog, G. G. Ross and J. W. F. Valle, Phys. Lett. B **150**, 142 (1985).
- [7] R. Hempfling, Nucl. Phys. B **478**, 3 (1996); M. Nowakowski and A. Pilaftsis, Nucl. Phys. B **461**, 19 (1996); A. S. Joshipura and M. Nowakowski, Phys. Rev. D **51**, 2421 (1995); T. Banks, Y. Grossman, E. Nardi and Y. Nir, Phys. Rev. D **52**, 5319 (1995); H. P. Nilles and N. Polonsky, Nucl. Phys. B **484**, 33 (1997).
- [8] A. G. Akeroyd, *et.al.*, Nucl. Phys. B **529** (1998) 3; A. Abada, S. Davidson and M. Losada, Phys. Rev. D **65** (2002) 075010; M. A. Díaz, J. Ferrandis, J. C. Romao and J. W. F. Valle, Phys. Lett. B **453** (1999) 263; S. Y. Choi, E. J. Chun, S. K. Kang and J. S. Lee, Phys. Rev. D **60** (1999) 075002; A. G. Akeroyd, M. A. Díaz and J. W. F. Valle, Phys. Lett. B **441** (1998) 224; O. Haug, J. D. Vergados, A. Faessler and S. Kovalenko, Nucl. Phys. B **565** (2000) 38; M. A. Díaz, E. Torrente-Lujan and J. W. F. Valle, Nucl. Phys. B **551** (1999) 78; A. S. Joshipura, R. D. Vaidya and S. K. Vempati, Nucl. Phys. B **639** (2002) 290; S. K. Kang and O. C. W. Kong, Phys. Rev. D **69** (2004) 013004.
- [9] D. F. Carvalho, M. E. Gomez and J. C. Romao, Phys. Rev. D **65** (2002) 093013; M. A. Díaz, J. Ferrandis, J. C. Romao and J. W. F. Valle, Nucl. Phys. B **590** (2000) 3; Y. Grossman and H. E. Haber, Phys. Rev. D **63** (2001) 075011; M. A. Díaz, J. Ferrandis and J. W. F. Valle, Nucl. Phys. B **573** (2000) 75; R. Kitano and K. y. Oda, Phys. Rev. D **61** (2000) 113001; A. G. Akeroyd, E. J. Chun, M. A. Díaz and D. W. Jung, Phys. Lett. B **582** (2004) 64; F. Takayama and M. Yamaguchi, Phys. Lett. B **476** (2000) 116.
- [10] M. Hirsch, *et.al.*, Phys. Rev. D **62**, 113008 (2000) [Erratum-ibid. D **65**, 119901 (2002)]; J. C. Romão, *et.al.*, Phys. Rev. D **61**, 071703 (2000).

- [11] F. De Campos, M. A. Díaz, O. J. P. Éboli, M. B. Magro and P. G. Mercadante, Nucl. Phys. B **623**, 47 (2002); M. A. Díaz, R. A. Lineros and M. A. Rivera, Phys. Rev. D **67** (2003) 115004.
- [12] M. A. Díaz, J. C. Romão and J. W. F. Valle, Nucl. Phys. B **524**, 23 (1998).
- [13] J. M. Mira, E. Nardi, D. A. Restrepo and J. W. F. Valle, Phys. Lett. B **492**, 81 (2000).
- [14] J. C. Romão, F. de Campos, M. A. García-Jareño, M. B. Magro and J. W. F. Valle, Nucl. Phys. B **482**, 3 (1996).
- [15] M. A. Díaz, arXiv:hep-ph/9712213.
- [16] M. A. Díaz, M. Hirsch, W. Porod, J. C. Romão and J. W. F. Valle, Phys. Rev. D **68**, 013009 (2003).
- [17] A. Djouadi, J. L. Kneur and G. Moultaka, arXiv:hep-ph/0211331.
- [18] J. Abdallah *et al.* [DELPHI Collaboration], Eur. Phys. J. C **34** (2004) 145 [arXiv:hep-ex/0403047].
- [19] M. B. Magro, F. de Campos, O. J. P. Éboli, W. Porod, D. Restrepo and J. W. F. Valle, JHEP **0309**, 071 (2003).
- [20] W. Porod and P. Skands, arXiv:hep-ph/0401077.
- [21] M. Hirsch and W. Porod, Phys. Rev. D **68** (2003) 115007; A. Bartl, M. Hirsch, T. Kerner, W. Porod and J. W. F. Valle, JHEP **0311** (2003) 005; D. Restrepo, W. Porod and J. W. F. Valle, Phys. Rev. D **64** (2001) 055011; D. W. Jung, S. K. Kang, J. D. Park and E. J. Chun, arXiv:hep-ph/0407106; Phys. Rev. D **66** (2002) 073003; M. A. Díaz, D. A. Restrepo and J. W. F. Valle, Nucl. Phys. B **583** (2000) 182; A. Belyaev, M. H. Genest, C. Leroy and R. R. Mehdiev, arXiv:hep-ph/0401065.
- [22] Work in preparation.

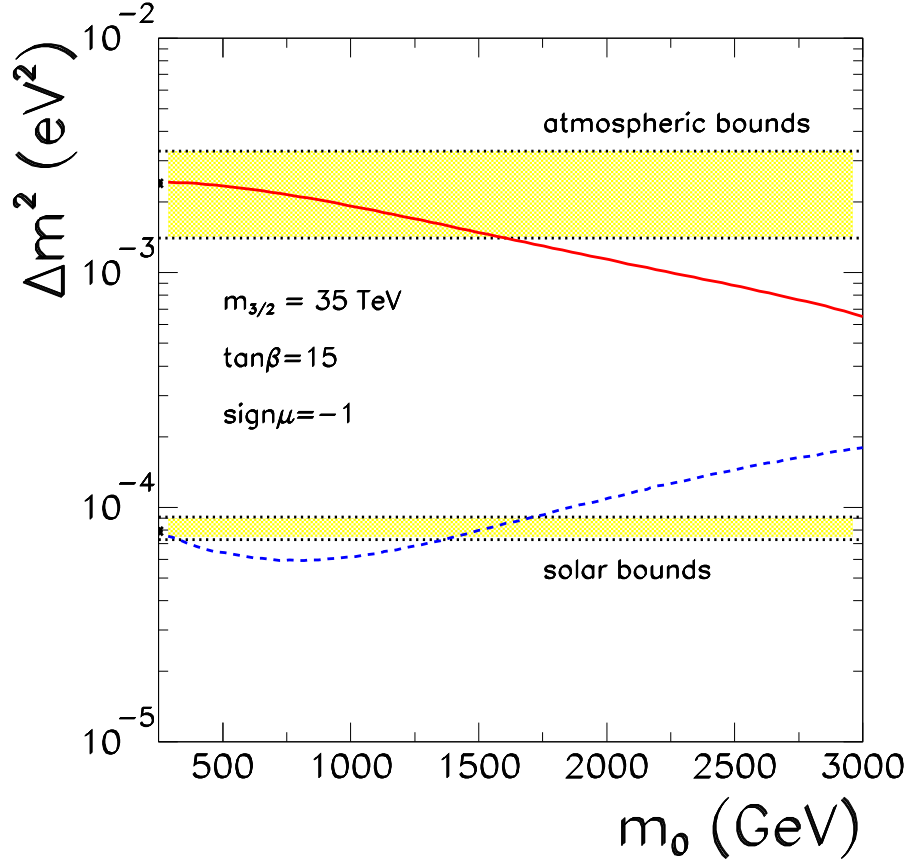


FIG. 1: The red solid (blue hashed) line stands for the predicted atmospheric (solar) mass squared difference as a function of the scalar mass m_0 for $m_{3/2} = 35$ TeV, $\tan\beta = 15$, and $\text{sign}(\mu) < 0$ and for the BRpV parameters given in (4.2). The allowed 3σ atmospheric (solar) mass squared difference is represented by the upper (lower) horizontal yellow band. Our reference point is represented by a star on the left of the plot.

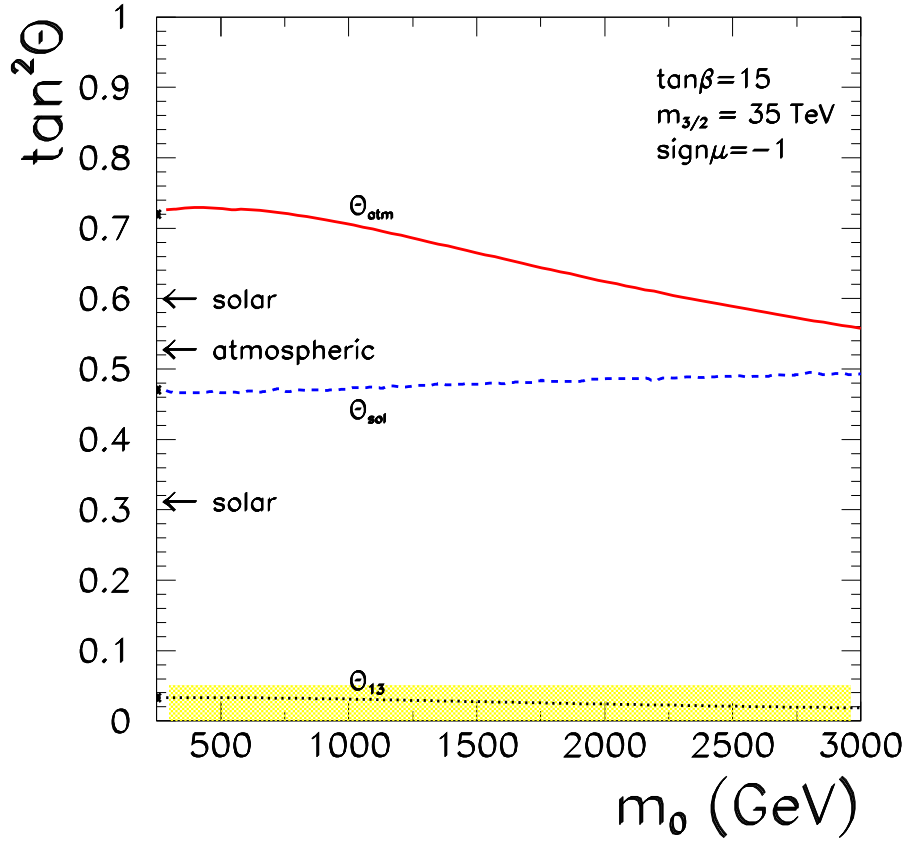


FIG. 2: Predictions of the AMSB–BRpV model for the atmospheric, solar, and θ_{13} mixing angles as a function of the scalar mass m_0 for the same parameters as in Fig. 1. The upper and lower 3σ bounds on the solar mixing angle and the 3σ lower bound on the atmospheric mixing angle are marked by the arrows while the yellow horizontal band states for the θ_{13} allowed region. Our reference point is represented by a star on the left of the plot.

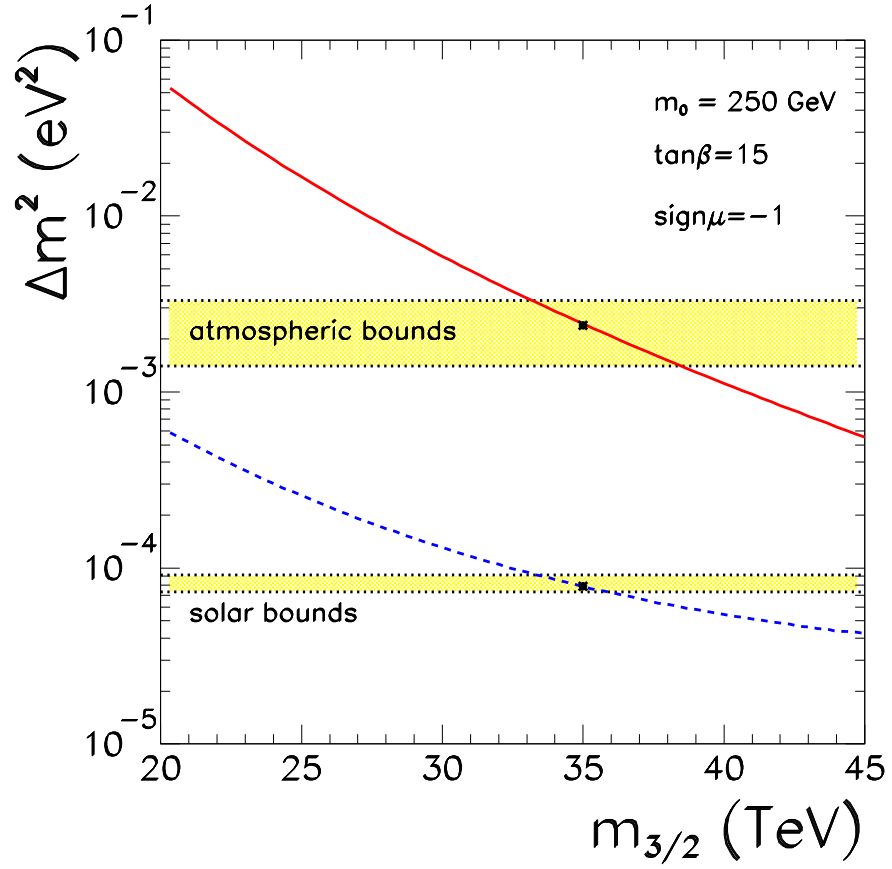


FIG. 3: Atmospheric (solid line) and solar (dashed line) mass squared differences as a function of the gravitino mass $m_{3/2}$. The remaining parameters assume the value of our reference point and the conventions are the same of Fig. 1.

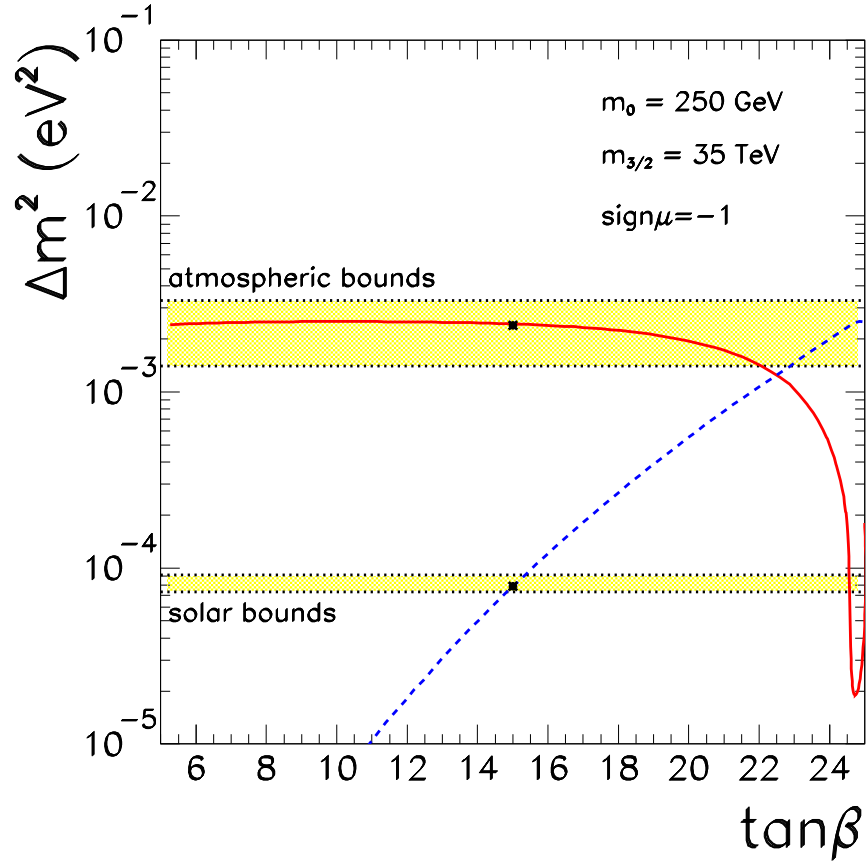


FIG. 4: Atmospheric (solid line) and solar (dashed line) mass squared differences as a function of $\tan \beta$. The remaining parameters assume the value of our reference point and the conventions are as in Fig. 1.

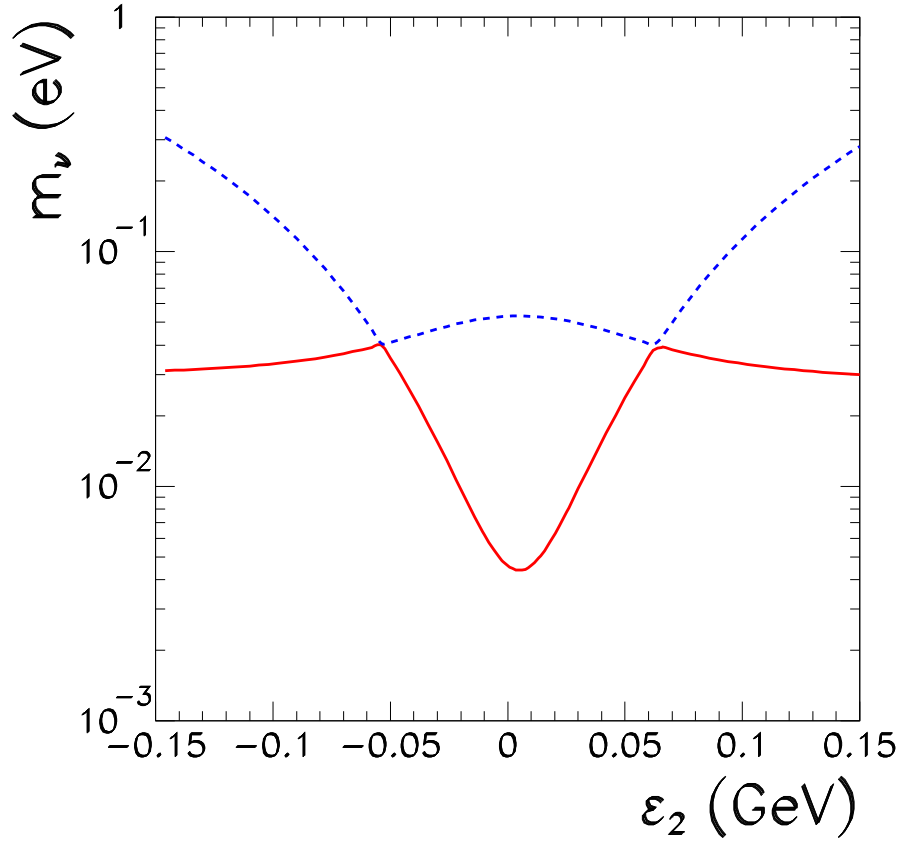


FIG. 5: Eigenvalues of the effective neutrino mass matrix as a function of ϵ_2 with the other parameters fixed at the reference point. The smallest eigenvalue is always smaller than 5×10^{-5} eV.

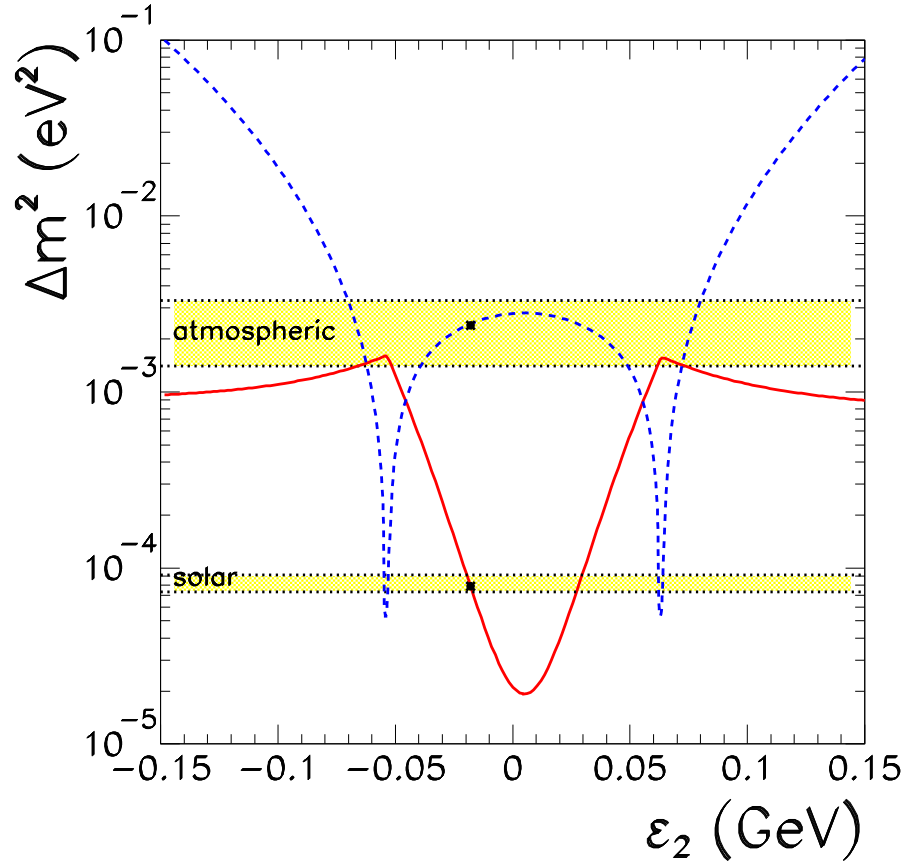


FIG. 6: The red solid (blue dashed) line stands for the atmospheric (solar) mass squared difference as a function of ϵ_2 with the remaining parameters fixed at their reference value. The allowed 3σ atmospheric (solar) mass squared difference is represented by the upper (lower) horizontal yellow band. Our reference point is represented by a star.

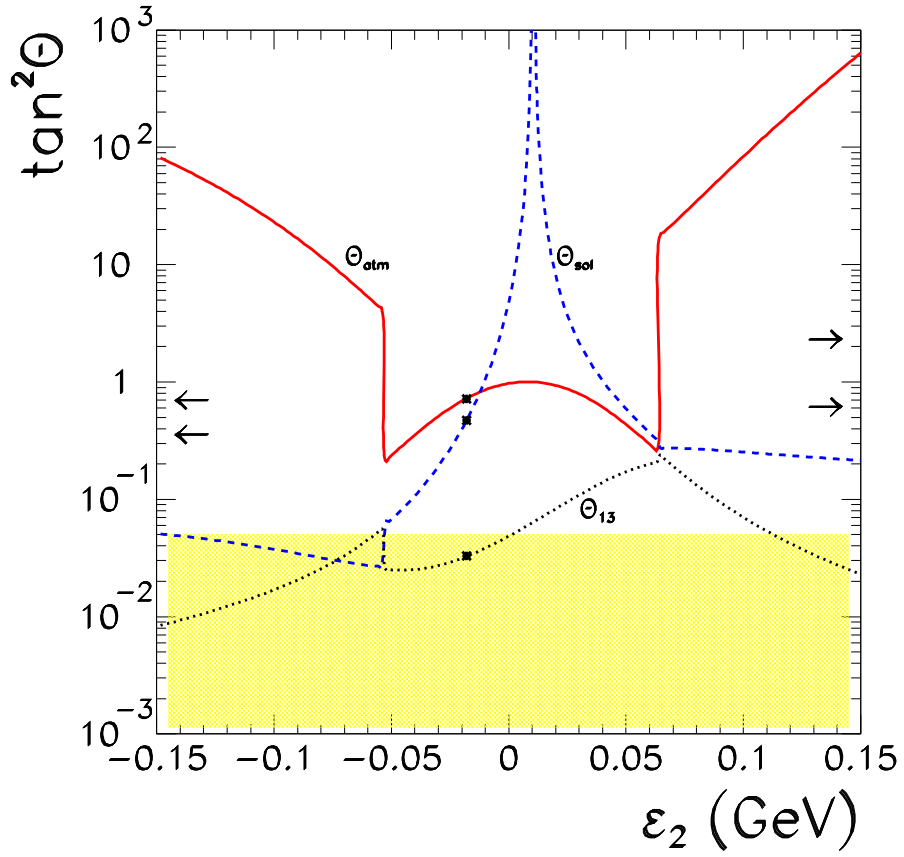


FIG. 7: The solid (dashed, dotted) line stands for the $\tan^2 \theta_{\text{atm(solar,13)}}$ as a function of ϵ_2 with the remaining parameters fixed at their reference value. The arrows on the right (left) of the figure indicate the 3σ bounds for atmospheric (solar) neutrinos. The CHOOZ allowed region for $\tan \theta_{13}$ is represented by the horizontal yellow area. Our reference point is marked by a star.

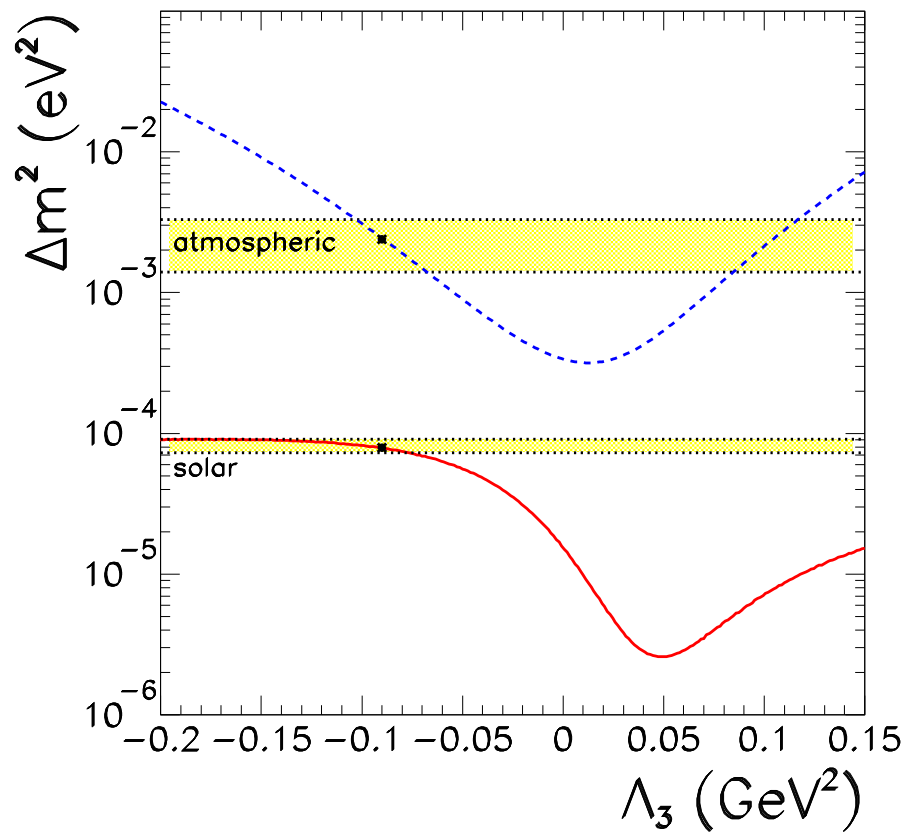


FIG. 8: The solid (dashed) line stands for the atmospheric (solar) mass squared difference as a function of Λ_3 with the remaining parameters fixed at their reference value. The upper (lower) shaded area corresponds to the 3σ allowed region for the atmospheric (solar) mass squared difference. Our reference point is represented by a star.

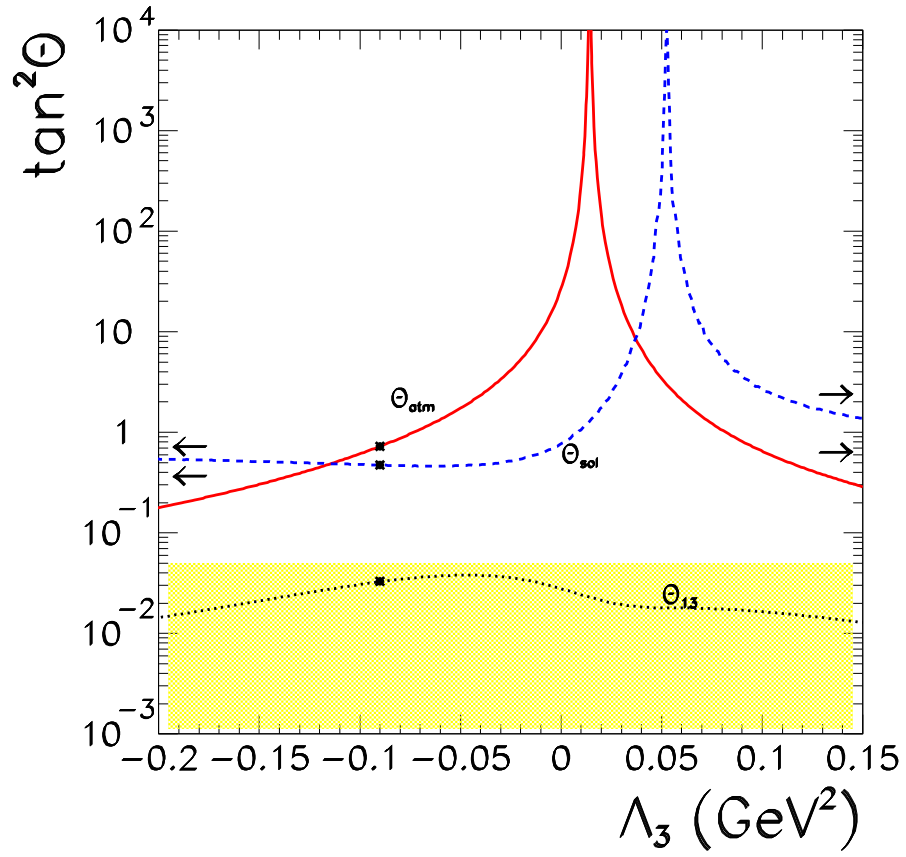


FIG. 9: Mixing angles as a function of Λ_3 . The conventions are the same of Fig. 7.